Aperture effects in 2.5-D Kirchhoff migration

Thomas Hertweck, Christoph Jäger, Alexander Goertz

Geophysical Institute, Karlsruhe University, Hertzstr. 16, 76187 Karlsruhe, Germany

{Thomas.Hertweck,Christoph.Jaeger,Alexander.Goertz}@gpi.uni-karlsruhe.de

and

Jörg Schleicher

Dept. of Applied Math., IMECC-UNICAMP, C.P.6065, 13081-970 Campinas (SP), Brazil

js@ime.unicamp.br

ABSTRACT

Seismic images obtained by Kirchhoff time or depth migration are always accompanied by some artifacts known as “migration noise”, “migration boundary effects”, or “diffraction smiles”, which may severely affect the quality of the migration result. Most of these undesirable effects are caused by a limited aperture if the algorithms make no special disposition to avoid them. Likewise, strong amplitude variation along reflection events may also cause similar artifacts. All these effects can be explained mathematically by means of the Method of Stationary Phase. However, such a purely theoretical explication is not always easy to understand for applied geophysicists. By relating the terms of the stationary-phase approximation to simple geometrical situations, a more physical interpretation of the migration artifacts can be obtained. A simple numerical experiment for post-stack (zero-offset) data indicates the problem and helps to develop an intuitive understanding of the effects and the methods to avoid them.

INTRODUCTION

Since the early work of Hagedoorn (1954), migration concepts have strongly improved and are now an important tool in the world of seismic imaging, either as prestack or poststack time and depth migration (see, e.g., Yilmaz, 2001). Hagedoorn's original (graphical) migration scheme using surfaces of maximum convexity was later related to the wave equation and became familiar as "Kirchhoff migration" (Schneider, 1978). The name was chosen with regard to the "Kirchhoff integral", which is used to describe the (forward) propagation of seismic waves within a given depth model. Since the Kirchhoff integral by itself cannot be used to solve the inverse problem, i.e., to describe backward propagation, Kirchhoff migration was introduced as its adjoint operation that describes the forward propagation of the recorded wavefield in the reverse direction. This turns out to be a very good approximation to backward propagation as long as evanescent waves can be neglected.

Kirchhoff migration treats each depth point M on a sufficiently dense grid like a diffraction point. In an a-priori given macrovelocity model, the relevant part of the Green's function of a point source at any single diffraction point M in the depth domain is calculated. The kinematic part of this Green's function is the configuration-specific diffraction-traveltime surface, also called "Huygens surface".

The amplitudes of the input seismograms (or, to be more specific, of their derivatives) are stacked along the Huygens surface and assigned to the depth point M. This explains why the Kirchhoff migration scheme is also called a "diffraction stack". If so desired, the effect of geometrical spreading can be removed from the output amplitudes by multiplying the data during the stack with a true-amplitude weight factor that is calculated from the dynamic part of the Green's function.

Ideally, the extent of the Huygens surfaces, that is, the migration aperture, should be limitless so that no contributions due to the abrupt truncation of the sum occur. In practice, of course, the aperture is always limited by the region over which seismic data have been acquired. In other words, because of the finiteness of the survey area, Kirchhoff migration will always be a "limited aperture migration" (LAM) (Sun, 1998).

This is, however, not the only reason why we have to deal with the effects of a finite migration aperture. In practial migration implementations, even ranges of source and receiver positions might be excluded where data actually have been acquired. Such a procedure can be advantageous because

- less traces to sum leads to a speedup of the whole migration process,
- a smaller operator excludes steeper dips, which helps to avoid operator aliasing (see, e.g., Abma et al., 1999),
- less summation of data away from the signal reduces the stacking of unwanted noise.

For the best possible reduction of aliasing and noise as well as the best computational efficiency, one would like to use a model-based aperture restriction, i.e., one would like to make use of the (projected) Fresnel zone (see, e.g., Schleicher et al., 1997; Sun and Bancroft, 2001). Unfortunately, it is difficult to determine the exact center and size of the Fresnel zone for each depth point prior to or during migration. A reasonable compromise between accuracy and practicability is to specify a

common maximum migration aperture radius or a maximum stacking operator dip. These aperture reductions lead to dip-restricted migration operators as, for example, a 45° migration. With these kinds of operators, higher dips cannot be imaged. In regions where dips are known to be restricted, this is a very convenient way of reducing aliasing and improving computational efficiency at the same time. It should, however, be kept in mind that close to the maximum dip, these dip-restricted migration operators will achieve only kinematically correct images (see, e.g., Schleicher et al., 1997; Sun, 1998). For true-amplitude migration, the maximum operator dip must always be chosen somewhat larger than the maximum reflector dip to be imaged.

The fact that the migration aperture is limited causes artifacts known as migration noise, boundary or aperture effects, or migration smiles. In this paper, we relate the mathematical explanation of the migration artifacts by means of the Method of Stationary Phase (see, e.g., Bleistein, 1984; Sun, 1998; Bleistein et al., 2001) to simple geometrical situations. This more physical interpretation leads to a more intuitive insight into these effects. Of course, since the stacking operations are the same in Kirchhoff time and depth migration, the corresponding artifacts are conceptually identical in both processes. Thus, we restrict our present discussion to Kirchhoff depth migration. It should, however, be kept in mind that everything said and shown in this paper with respect to an image in depth holds in the same way for an image in time.

KIRCHHOFF MIGRATION

Mathematically, the Kirchhoff migration process is expressed as an integration over the recorded wavefield and reads in 3-D (Tygel et al., 1996)

$$V(M) = -\frac{1}{2\pi} \iint\limits_{A} d\xi_1 \, d\xi_2 \; W_{DS}(\vec{\xi}, M) \; \frac{\partial U(\vec{\xi}, t)}{\partial t} \bigg|_{t=\tau_D(\vec{\xi},M)} , \tag{1}$$

where $V(M)$ is the value assigned to one diffraction point M in the depth domain after migration and $U(\vec{\xi}, t)$ denotes the data in the time domain (seismograms). These data are assumed to consist of analytic traces which allows the handling of complex reflection coefficients (supercritical reflections) and possible caustics along the ray paths. An analytic trace is formed by the actual trace recorded in the field as the real part and its Hilbert transform as the imaginary part. The vector $\vec{\xi} = (\xi_1, \xi_2)$ is the so-called configuration parameter vector and represents the trace position. Sources and receivers are grouped into pairs, whose locations are described as a function of $\vec{\xi}$. The actual form of this function depends on the measurement configuration. The migration aperture A is the area over which $\vec{\xi}$ varies to cover all source-receiver pairs used in the stack.

The factor $W_{DS}(\vec{\xi}, M)$ is a true-amplitude weight function which may (true-amplitude migration) or may not (purely kinematic migration) be included in the migration scheme. The stacking surface $\tau_D(\vec{\xi}, M)$ is the above-mentioned Huygens surface. The time derivative is needed in order to correctly recover the source pulse (Newman, 1975).

We assume that at least one reflection event is present in the seismic data $U(\vec{\xi}, t)$. Then, these data can be described by zero-order ray theory (see, e.g., Červený, 2001) as

$$U(\vec{\xi}, t) = R_c \frac{\mathcal{B}}{\mathcal{L}} \cdot F(t - \tau_R) \; , \tag{2}$$

where R_c denotes the angle-dependent reflectivity, $\mathcal{L}$ symbolizes the point-source geometrical spreading factor, and $\mathcal{B}$ describes all other effects on the amplitude, such as source strength, source

and receiver coupling, transmission loss and attenuation in the reflector overburden, to name a few. Moreover, $F(t)$ is the analytic source wavelet which is shifted to the arrival time τ_R (reflection traveltime). A seismic trace with several (primary) events may be described by superposition of individual seismic events of the type of equation (2).

To enable a Fourier transform, we introduce the time t as an additional parameter in equation (1). This is nothing but a mathematical trick that can be undone by setting $t = 0$. Then, we can rewrite equation (1) in the frequency domain as

$$\hat{V}(M,\omega) = -\frac{i\omega}{2\pi}\,\hat{F}(\omega) \iint\limits_{A} d\xi_1\, d\xi_2\, W_{DS}(\vec{\xi}, M)\, R_c \frac{\mathcal{B}}{\mathcal{L}}\, e^{i\omega\tau_{dif}}\ , \tag{3}$$

where $\hat{F}(\omega)$ and $\hat{V}(M,\omega)$ denote the Fourier transforms of $F(t)$ and $V(M,t)$, respectively. Moreover, $\tau_{dif}(\vec{\xi}, M)$ is the difference between the diffraction and reflection traveltimes, i.e., $\tau_{dif} = \tau_D - \tau_R$.

In 2.5-D, i.e., when the medium does not vary with respect to the coordinate perpendicular to the seismic line (crossline direction), the out-of-plane ξ_2-integration in equation (3) can be evaluated analytically. Since all data acquired on lines parallel to the actual seismic line would be identical, the migration aperture A can be assumed to be infinite in the ξ_2-direction. Kirchhoff migration then reduces to an in-plane stack over the aperture interval (a, b) in the ξ_1-direction covered by the seismic line. Since ξ_1 is now the only integration variable, we can drop the index 1 to write the 2.5-D Kirchhoff migration integral as

$$\hat{V}(M,\omega) = \sqrt{\frac{-i\omega}{2\pi}}\,\hat{F}(\omega) \int\limits_{a}^{b} d\xi\, W_{DS}^{(2.5)}(\xi, M)\, R_c \frac{\mathcal{B}}{\mathcal{L}}\, e^{i\omega\tau_{dif}}\ , \tag{4}$$

where $W_{DS}^{(2.5)}$ is the 2.5-D weight factor that guarantees true amplitudes in this 1-D stack. It is composed of the 3-D weight factor and the result of the analytic solution of the out-of-plane integral.

THE METHOD OF STATIONARY PHASE

In general, the integrals in equation (3) and the remaining integral in equation (4) cannot be solved analytically. The Method of Stationary Phase provides a way of analyzing their main contributions. Although in principle a high-frequency approximation, the Method of Stationary Phase yields highly accurate predictions of the migration results in the seismic frequency range. Mathematically, the prerequisites for applying the Method of Stationary Phase are implicitly fulfilled, since we perform all calculations within the framework of zero-order ray theory which is strictly valid only for high frequencies.

For simplicity, we restrict the following analysis to the 2.5-D case. Conceptually, there is no difference in the application of the Method of Stationary Phase to the double integral for 3-D migration. The qualitative discussion involves the same arguments and leads to the same conclusions. The quantitative analysis is similar but slightly more complicated, mainly resulting in a different amplitude behavior of the artifacts.

Reducing it to its basic structure, the integral in equation (4) can be written in the form

$$I(\omega) = \int_a^b f(\xi) e^{i\omega q(\xi)} d\xi \ . \tag{5}$$

The Method of Stationary Phase is based on the observation that for high frequencies, i.e., for large values of ω, the factor $e^{i\omega q(\xi)}$ oscillates very rapidly, thus covering full periods in very small intervals of ξ. If $f(\xi)$ is not itself an oscillating function, its values do not strongly vary in any such interval. Thus, the integration over a full period of $e^{i\omega q(\xi)}$ yields approximately zero and does not contribute to the overall value of the integral. The only regions where $e^{i\omega q(\xi)}$ does not oscillate are those where the phase function $q(\xi)$ remains approximately constant or *stationary*. Mathematically, points of stationary phase are those where the phase function $q(\xi)$ has a horizontal tangent, i.e., a vanishing derivative. Non-negligible contributions to integral (5) are, therefore, to be expected from the vicinity of these points. Further contributions to integral (5) are to be expected from the boundaries of the integration interval because there, the integration generally does not cover a full period of $e^{i\omega q(\xi)}$.

To illustrate the above observations, we consider the migration of zero-offset data from a simple earth model with a horizontal reflector at a depth of 1 km. For a point M at $x = 3$ km on the reflector and a frequency of 30 Hz, Figure 1(a) and (b) show the phase and amplitude of the integrand in equation (4), respectively, as a function of ξ. The real part of the exponential function is depicted in part (c) of that figure. Note that this function strongly oscillates everywhere except in the vicinity of the point where the phase is stationary. Finally, part (d) shows the real part of the full integrand function. It is evident that the amplitude modulation does not alter the oscillatory character of the integrand function.

Let us now discuss integral (5) in a more quantitative way. In our case, the phase function q is the difference between the diffraction and reflection traveltime curves, τ_{dif}. Thus, the real part of the integrand function (Figure 1(d)) has zeroes at

$$|\tau_{dif}| = |\tau_D - \tau_R| = n\,\frac{\pi}{\omega} = n\,\frac{T}{2} \ , \tag{6}$$

where $T = 2\pi/\omega$ is the period of the monofrequency wave under consideration. Equation (6) is equivalent to the definition of the boundary of the nth Fresnel zone (see, e.g., Červený and Soares, 1992). Therefore, the alternating zones of negative and positive amplitude of the integrand function are physically equivalent to the Fresnel zones[1].

Now, consider an integration of the function $f \cdot \exp(i\omega q)$ from the center (where $\tau_D = \tau_R$) to the sides. At first, this sums up positive contributions from the first Fresnel zone, ending at the first zero in either direction. Subsequent Fresnel zones, each ending at the next zero, will add purely negative or positive contributions to integral (5). In other words, Fresnel zones with odd numbers contribute positively to the integral while Fresnel zones with even numbers contribute negatively. Because of the above observation that an integration over a full period, i.e., over two consecutive Fresnel zones, yields approximately zero, it becomes clear why the principal contribution to integral (5) will stem from the vicinity of the stationary point. Hence, an integration over only the first Fresnel zone

[1]To be exact, what is involved in Kirchhoff migration is the projected Fresnel zone in the data space (Hubral et al., 1993). The true Fresnel zone in depth can be observed in the Kirchhoff modeling integral. Conceptually, however, there is no difference.

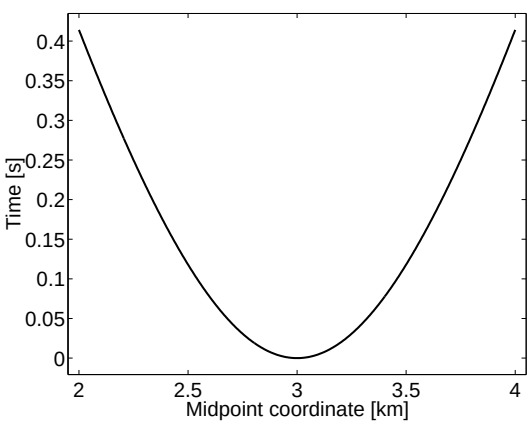

(a) Phase function $q(\xi)$

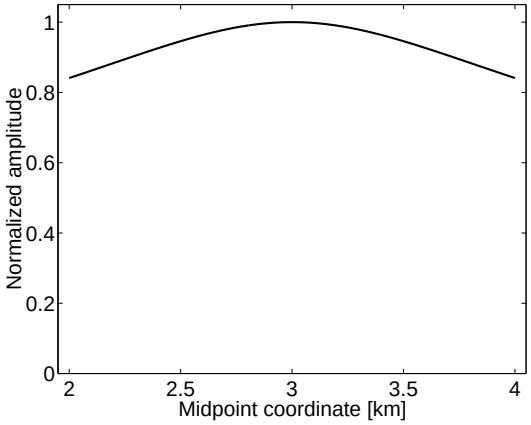

(b) Amplitude function $f(\xi)$

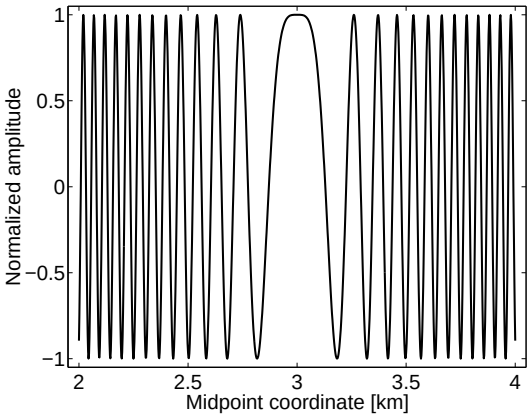

(c) Real part of exponential function $e^{i\omega q}$

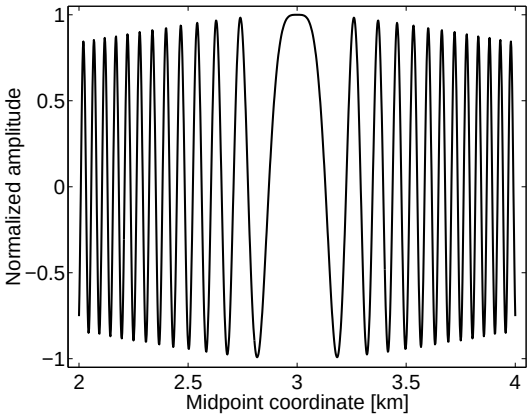

(d) Real part of integrand function

Figure 1: Illustration of the integrand in equation (4). (a) Phase function $q(\xi)$. (b) Amplitude function $f(\xi)$. (c) Real part of the exponential function $\exp(i\omega q)$. (d) Real part of the complete integrand function $f \cdot \exp(i\omega q)$.

already provides a very good approximation of the total integral. On the other hand, its full value cannot be recovered, if the integration interval does not cover the first Fresnel zone completely.

It has to be noted, however, that the above discussion holds strictly only for a monofrequent signal. For a transient, band-limited signal, one has to replace the half-period $T/2$ in equation (6) by some estimate of the the wavelet length τ_W.

In Appendix A, we shortly summarize the analysis of the migration integral (5) by means of the Method of Stationary Phase under the assumption of a single, simple and isolated point of stationary phase. The result of this analysis up to second order in $1/\sqrt{\omega}$ is

$$I(\omega) \quad \simeq \quad f(\xi^*)e^{i\omega q(\xi^*)}\sqrt{\frac{2\pi}{-i\omega q''(\xi^*)}} + \frac{1}{i\omega}\left[\frac{f(b)}{q'(b)}e^{i\omega q(b)} - \frac{f(a)}{q'(a)}e^{i\omega q(a)}\right] , \tag{7}$$

where the prime denotes the derivative with respect to ξ. For high frequencies, these expressions describe the major contributions to the final migrated image. The first term stems from the sta-

tionary point ξ^* of the phase $q = \tau_D - \tau_R$, that is, the tangency point between the Huygens and reflection traveltime curves, and forms the actual migrated image of the reflector(s). In general, this contribution will be the dominant part of the total migrated section. The second term comes from the endpoints of the integration/stacking operator. It is this second contribution that describes the main migration artifacts. Because of the higher order in $1/\sqrt{\omega}$, its amplitudes generally will be lower than those of the reflector image. Note, however, that under certain circumstances these effects can be as strong as (or even stronger than) a reflector image.

Apart from the edges of the acquisition aperture and the stacking operator, also discontinuities along the reflection events in the seismic data may cause this kind of endpoint contributions. These discontinuities affect the integral as if acting piecewise on the data. In other words, we may say that "artificial" endpoints are created which cause the additional aperture effects. There are several situations in which such discontinuities can occur. They can be caused by illumination problems or missing traces in the data. In this case, the migration smiles can even be desirable as they may help to reconstruct reflector continuity. Moreover, amplitude variations along the reflection event, which may be due to focusing and defocusing of the reflected wave, can cause similar effects as endpoints.

It is to be remarked that migration artifacts due to a limited aperture, illumination problems, or missing traces are inherent to seismic migration, independently of the actual migration scheme employed. Artifacts due to strong amplitude variations and focusing effects are, however, a consequence of Kirchhoff migration and can be largely reduced with other migration schemes such as, e.g., finite-difference wave-equation migration.

In contrast to the data boundaries, actually ending reflectors in the earth do not provoke migration smiles. In this case, edge diffractions are present in the seismic data that are collapsed by migration into the endpoint of the reflector. Because of the diffractions, the reflection event in the data has no actual endpoint but dies off over a larger number of traces. In this way, endpoint contributions are suppressed. The latter observation already points towards a well-known way of suppressing migration artifacts: tapering. We will discuss this in a later section.

GEOMETRICAL EXPLANATION OF THE APERTURE EFFECTS

The migration aperture effects are most easily explained by means of a simple numerical experiment for poststack data. The model consists of two half-spaces separated by a horizontal interface. The velocities in the upper and lower half-spaces are $v_p^{(1)} = 2$ km/s and $v_p^{(2)} = 3$ km/s, respectively, and the shear wave velocities are given by $v_s = v_p/\sqrt{3}$. The density is constant in the whole model. The zero-offset seismogram was generated by dynamic ray tracing using a zero-phase Ricker wavelet with 20 Hz, a time sampling of $dt = 1$ ms and a trace distance of $\Delta\xi = 5$ m. It was migrated with a 2.5-D Kirchhoff true-amplitude depth migration scheme on a dense grid ($dx = 10$ m, $dz = 2$ m) using the true velocity.

For this simple model, the stacking operator is given by a hyperbola. We limited its spatial extent to 800 m with respect to the horizontal coordinate of the apex. In this way, the number of traces contributing to the stack for each depth point was 320. The migration target zone was placed at the end of the survey line so as to show the boundary effects. The resulting migrated image is depicted in Figure 2. Note that no effort was made to enhance or reduce the migration artifacts.

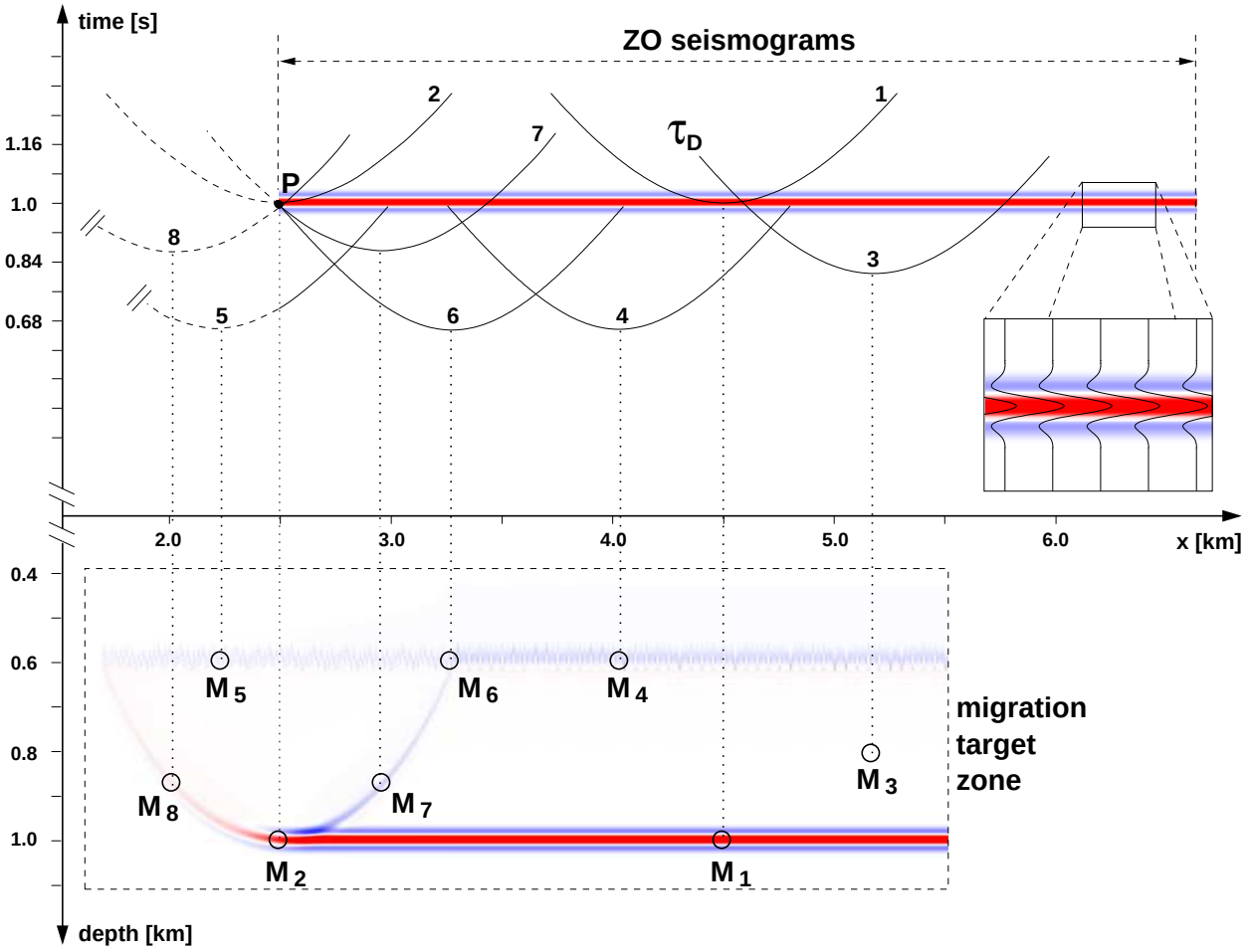

Figure 2: ZO seismogram and corresponding depth image after poststack migration. Several characteristic depth points M_j and their pertinent stacking operators are shown. These are used to give a simple geometrical explanation of the limited aperture migration effects.

By means of Figure 2, we are now going to discuss the boundary effects from a geometrical point of view, which allows us to gain a more intuitive insight. We then relate them to the above discussion of the interference in integral (5) and to the result of its stationary-phase evaluation as given by equation (7). For this purpose, we discuss the position of the Huygens curves pertaining to a series of characteristic depth points M_1 to M_8.

Points on the reflector: M_1

The actual reflector (which is unknown prior to migration) is built up by depth points like M_1. The pertinent Huygens curve is tangent to the reflection traveltime curve. Thus, amplitudes gathered along such a curve sum up coherently and provide high stacking results that are assigned to the corresponding depth point. Note that in general, for laterally inhomogeneous media, the tangency point does not coincide with the apex of the stacking curve. To relate this physical explanation to our earlier considerations of the Method of Stationary Phase, we identify these tangency points with the "points of stationary phase". The value assigned to M_1 is mathematically described by the first term in equation (7). No boundary effects are present because the input data at the endpoints of the stacking operator, which correspond to the limits of integration a and b in equation (4), are

zero. Of course, in practice there will always be some endpoint contributions because of the noise inherent in the seismograms.

Points on the reflector boundary: M_2

The point M_2 represents the boundary of the migrated reflector image. The Huygens curve of this point is, in principle, equivalent to the one of point M_1. However, since the stationary point is located directly at the margin of the ZO gather, only half the operator is within the data volume. Thus, summing up along the stacking curve results in an amplitude value which is half of the value assigned to M_1. This coincides with the stationary-phase analysis for the case when the stationary point falls on the boundary of the integration interval. Then, the left-hand-side integral in equation (A-7) extends only from ξ^* to infinity, which, due to symmetry, results in half the right-hand-side value. Thus, the leading term in equation (7) is divided by 2.

Points off the reflector: M_3

Points like M_3 represent the majority of diffraction points within the target zone. They have Huygens curves which completely cross the reflection signal. Summing up amplitudes along such operators leads to low values due to destructive interference. From a mathematical point of view, the point of stationary phase (i.e., where the traveltime and Huygens curves have the same time dip) as well as the endpoints of the operator are outside the signal. Therefore, both terms in equation (7) are zero.

Migration artifacts caused by the finite stacking operator: M_4**,** M_5**, and** M_6

For points like M_4, the endpoints of the stacking operator lie within the reflection signal. Because of the limited aperture, the stack does not sum up all the data necessary for complete destructive interference in the same way as it does for point M_3. Thus, the migration output at M_4 is not as low as that for point M_3. In consequence, a migration artifact appears in parallel to the actual reflector. With increasing size of aperture, the effect at M_4 moves away from the actual reflector and might be located outside of the target zone. Sun (1998) showed that this aperture effect completely separates from the reflector image if the aperture is larger than one Fresnel zone (see also Section “How to avoid aperture effects”).

The relationship of the above observations to the Method of Stationary Phase is straightforward. Like for point M_3, the point of stationary phase is outside the signal. However, the endpoints of the operator lie inside the signal. Therefore, the first term of equation (7) yields no contribution, but its second term predicts a non-zero migration output at M_4.

The situation at point M_5 is in principle equivalent to that at point M_4. However, as only one endpoint lies within the reflection signal (the other endpoint lies outside the data), the amplitude at M_5 is just half of that at M_4.

Point M_6 marks the transition between the two situations of points M_4 and M_5. The endpoint of its pertinent Huygens curve coincides with the boundary point P in the data, where the survey ends. It is for this reason that at M_6 the migration artifact splits into two effects. Additionally to

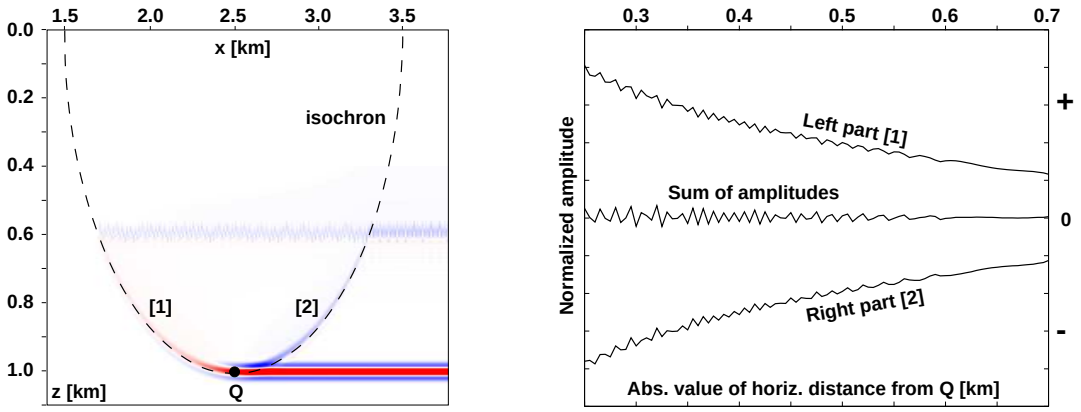

(a) Isochron

(b) Amplitudes along the artifact branches

Figure 3: Analysis of the migration smile. (a) Kinematically, it coincides with the isochron of the border point P of the data. (b) The sum of peak amplitudes of two opposite points on the isochron branches [1] and [2] yields approximately zero.

the limited-operator effect described above, a limited-data effect appears in the migrated traces.

Migration artifacts caused by the finite survey area: M_7 and M_8

The most prominent migration artifact is the "migration smile" represented by points M_7 and M_8. The pertinent Huygens curves cross the reflection signal exactly at the end of the survey line. In this way, the destructive interference is incomplete at one of the endpoints, thus leading to a non-negligible contribution.

It is worthwhile to observe that the position of the migration smile is given by the geometrical location of all points of the type of M_7 and M_8 whose Huygens curves cut the border point P of the reflection signal. Note that, because of the duality between the Huygens curve and the isochron (see, e.g., Tygel et al., 1995), this is the isochron of P. The resulting migration artifact follows this isochron, which is a half-circle for our constant-velocity zero-offset experiment as shown in Figure 3(a).

Observe the inverted polarity (red is positive, blue is negative) of the artifact between points M_7 and M_8. This can be explained with the help of the symmetry of the operator. The dashed part of the Huygens curve of M_7 that is outside the data is identical to the solid part of the Huygens curve of M_8 that is inside the data. Thus, the stack at M_8 will contribute with exactly that part of the data that is missing at M_7. The actual values of the migration results at points M_7 and M_8 depend on the form of the source wavelet as well as on the (half-)derivative applied in the migration process. However, the fact that these values are complementary to each other is independent of these conditions. For a better visualization of this complementarity, we have picked the peak amplitudes along both branches of the migration smile corresponding to points M_7 and M_8. When adding the amplitude of two opposite points from the two branches, we can verify in Figure 3(b) that the sum at M_7 and M_8 indeed yields zero (except, of course, for a numerical error).

Again, we can directly relate the above physical interpretation to the terms of the stationary-phase evaluation of the Kirchhoff-migration integral. Of course, the migration outputs at points M_7

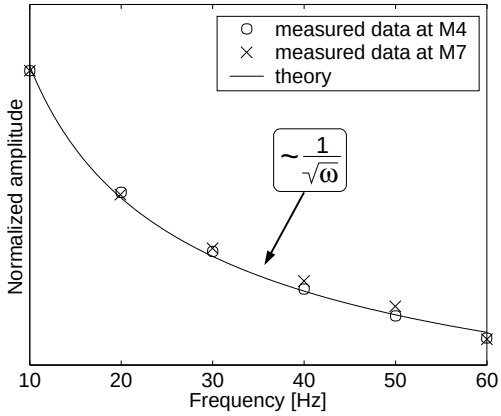

Figure 4: Frequency behavior of the boundary effects in 2.5-D. The amplitude at M_4 (circles) and M_7 (crosses) decays with $1/\sqrt{\omega}$ as predicted by the Method of Stationary Phase.

and M_8 are described by the second term in equation (7). The first term yields a zero contribution since the stationary point is outside the reflection signal as in the case of points M_3, M_4, M_5, and M_6. At both points, M_7 and M_8, the actual contribution stems from the lower integral limit, $a = 2500$ m. Since the Huygens curves of both points terminate at the same position, $f(a)$ is the same for both of them. So where is the inverted polarity? It's in the sign of the derivative, i.e., in our simple example the dip of the stacking curve, at the survey end. As we can easily observe in Figure 2 this sign is positive for M_8 but negative for M_7.

The Method of Stationary Phase evaluation allows for a more quantitative analysis of the migration smile. Using equation (7) and recalling the additional factor $\sqrt{\omega}$ in front of the integral in equation (4) (which stems from the time half-derivative in the original Kirchhoff migration integral), we see that the main contribution to the migration result will be frequency independent while the boundary effects will decay proportionally to $1/\sqrt{\omega}$. Figure 4 shows the amplitude of the migration output at points M_4 (circles) and M_7 (crosses) as a function of the dominant frequency of the source wavelet used in the modeling. The actually observed amplitudes follow almost exactly the predicted behavior (solid line).

Prestack Migration and Comparison with Sun (2000)

The reader might notice that the examples of "Limited Aperture Migration" (LAM) in Sun (2000) do not distinguish between the different types of migration artifacts as described above. The reason is quite simple: Sun uses a prestack migration example with a single shot only and, in addition, he shows only a single trace of the migration result in the center of the survey. In that case, only one artifact is visible, namely that due to the limited operator as represented above by points M_4 and M_5. Of course, both aperture effects are also present in prestack migration as can be seen in Figure 5. To construct this figure, the data were sorted into common-offset gathers and then migrated separately. The actual migration operator was limited to a maximum aperture radius of 0.8 km around its apex. The respective migration results are displayed in parallel planes to the front face of the cube, which is identical to the zero-offset migration shown in Fig. 2. Perpendicular to the front face is the offset axis. In this way, the side face of the cube is an image gather that depicts the same reflector point as obtained from migration of all offsets.

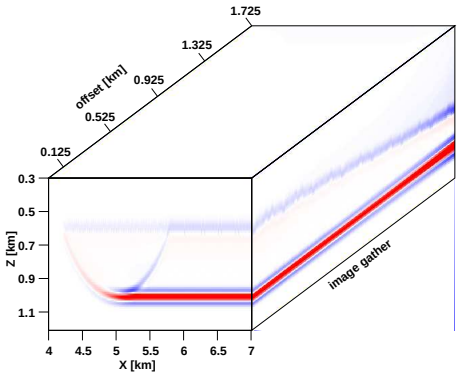

Figure 5: 2-D prestack migration of the same model used in the ZO example. The maximum aperture radius was 0.8 km. Both types of artifacts can be observed. The effect caused by the limited operator has a moveout in the image gathers.

As the operator moveout reduces with higher offset, the artifact due to the limited migration operator moves closer to the migrated reflection for large offsets. The isochron-type artifact due to the limited survey area moves along the x-axis in offset direction due to different reflector illumination for different offsets. Note that a post-migration stack can significantly reduce these migration artifacts, because of the mentioned moveout in the offset direction. In spite of that, in complex media some strong artifacts will generally remain visible in the final migrated section.

Boundary effects in 3-D

In 3-D, the physical conditions that cause boundary effects are the same as in 2.5-D, these being the ends of the seismic data and of the stacking operator. Therefore, the migration artifacts to be observed in 3-D Kirchhoff migration are conceptually the same as in 2.5-D. One will see the migration smile from the survey end as well as the effect due to the limited operator size. This is confirmed by a corresponding 2-D stationary-phase analysis of integral (1), which also reveals the two leading-order contributions to be those from the stationary point(s) and the integration limits.

However, the increase in dimension slightly changes the situation. The geometrical situation and, accordingly, the mathematical derivations are more complicated. The stacking operator is no longer a line but a surface and its boundary is not a point but a line. For that reason, the amplitude behavior of the artifacts can be different.

Figure 6 shows corresponding numerical results from a 3-D migration. The model and all its parameters are the same as for the above 2.5-D experiment, extending it identically into the third dimension. Indicated is the $1/\sqrt{\omega}$-behavior (solid line) together with the amplitudes of the 3-D migration artifacts at points that correspond to points M_4 and M_7 in Figure 2, here denoted in quotation marks, i.e., as "M_4" and "M_7". The amplitude of the artifact at point "M_7" decays with $1/\sqrt{\omega}$ (as in the 2.5-D case). However, the artifact built up by points like "M_4" shows almost no frequency dependence.

The observed amplitude behavior of both effects can be explained by the 2-D Method of Stationary Phase. However, it would go beyond the scope of this paper to enter into the mathematical details of 3-D migration artifacts and to comment on all similarities and differences to the 2.5-D situation. This will be the topic of a forthcoming paper on the 3-D case.

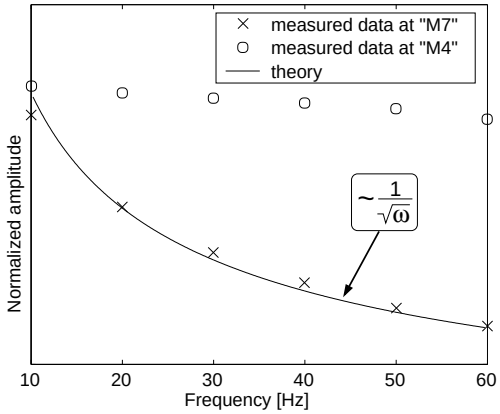

Figure 6: Amplitude behavior of the boundary effects in a 3-D migration. Circles: amplitudes at a point "M_4", crosses: amplitudes at a point "M_7", solid line: $1/\sqrt{\omega}$ behavior predicted by the Method of Stationary Phase for point "M_7".

HOW TO AVOID APERTURE EFFECTS

Above, we have already indicated that there is a well-known technique to reduce migration artifacts resulting from the limited migration aperture. All that has to be done is to avoid an abrupt end of the operator but let it die off over a couple of traces, i.e., apply a taper. This has to be done at two different places: Firstly, the input seismograms are tapered at the endpoints of the survey area. Secondly, the finite operator is not just truncated but also tapered at its endpoints. In terms of the stationary-phase solution (7), the values of $f(a)$ and $f(b)$ are artificially set to zero. This has to be done smoothly in order not to violate the underlying assumption of a slowly varying function $f(\xi)$. Then, this approach reduces the contributions of the operator endpoints and, thus, helps to obtain a migrated image with less migration artifacts.

When applying a taper, the fundamental question is over how many traces it should extend. On the one hand, the taper ought to be large enough not to violate the smoothness assumption so as to effectively suppress the artifacts. On the other hand, it should not be too large so as not to loose more information than necessary on the amplitudes at the survey ends or to stack unnecessary information at the operator ends. Sun (1998) suggests that in the same way as the stacking region should cover the first (projected) Fresnel zone, the taper region should extend over the second (projected) Fresnel zone around the stationary point. Unfortunately, this point cannot be estimated prior to or during migration. Therefore, we have to use once again a compromise to avoid the aperture effects.

To get an idea about the size of the taper region, we propose the following simple criterion for zero-offset (poststack) migration. As is well-known, to kinematically migrate all reflectors at depth z up to maximum dip angle θ_m, the stacking operator may be restricted to a radius of

$$r = z \tan \theta_m \ . \tag{8}$$

If the same reflectors are to be migrated dynamically correctly, the radius must be increased by the size $FZ(1)$ of the projected first Fresnel zone. As shown in Appendix B, $FZ(1)$ is given in the frequency domain by

$$FZ(n) = \frac{\sqrt{\frac{vznT}{2\cos\theta_m} + \left(\frac{nvT}{4}\right)^2}}{\cos\theta_m} \tag{9}$$

with $n = 1$, where v is the medium velocity and T the period of the considered monofrequency wave. Like in equation (6), the half-period $T/2$ has to be replaced by some estimate of the wavelet length τ_w, if formula (9) is to be applied in the time domain. According to Sun (1998), the artifacts are suppressed as well as possible, while affecting the amplitudes as little as possible, when the operator is increased by $FZ(2)$ instead of $FZ(1)$. The additional operator extension $FZ(2) - FZ(1)$ is the second projected Fresnel zone, over which the taper is to be applied. Of course, the formulas given above are strictly valid for constant velocity only. For inhomogeneous media, they can only be used as a "rule of thumb" to get a rough idea about the aperture size and the taper region.

Formula (9) can also be used to obtain an estimate for the size of the end-of-survey taper. By substituting $z = vt \cos\theta_m/2$ and setting $n = 1$, the size of the taper at two-way time t can be estimated. If a constant taper size is preferred, t can be replaced by the maximum time value in the data. Correspondingly, z in equation (9) can also be replaced by the maximum depth in the desired migrated image.

Figure 7 demonstrates the effect of tapering the input data and the stacking operator for different aperture and taper sizes.

Figure 7(a) shows the migrated reflector image when stacked with a dip-limited 0° migration operator using the optimal aperture of one projected Fresnel zone, without applying a taper. Both the migration artifacts due to the limited operator and survey area are present. As we can see, the optimal aperture guarantees the separation of the end effect from the reflector image, the amplitudes of which are also correct. Figure 7(b) shows the same migrated reflector image with the optimal taper applied. Both artifacts are almost completely eliminated. In Figure 7(c), we see the effect of a too small taper. Although both migration artifacts are reduced, they remain clearly visible. Finally, Figure 7(d) compares the amplitudes along the reflector image for different combinations of aperture and taper sizes. When the aperture is too small, not even the amplitudes far away from the data margins are correctly recovered (dotted line), although the optimal taper is used. When the optimal (or a larger) aperture is applied, all amplitude problems are restricted to the data margins. For too small a taper, the survey-end artifact is not completely removed (dashed line). Too large a taper destroys the amplitudes where they can be retrieved from the data (dash-dotted line). The optimal taper size is the one that eliminates all artifacts but recovers the amplitudes as close to the margins as possible (solid line).

The taper function used for the migration examples shown here is a two-sided Hanning window for both the operator and the end-of-survey taper. For comparison, we also tested a two-sided triangular window. The shapes of these functions are depicted in Sun (1998, 2000) for 2-D and 3-D. Both types of taper functions yield nearly identical results. The optimal values for the aperture and taper sizes were calculated by means of equation (9) with $z = 1$ km, $v = 2$ km/s, $\tau_w = 50$ ms, and $\theta_m = 0^\circ$, resulting in $FZ(1) = 320$ m and $FZ(2) = 458$ m. To test the effect of a too small and large aperture or taper size, respectively, the stacking region $FZ(1)$ and the taper region $FZ(2) - FZ(1)$ were halfed or doubled.

At this stage, let us point out that with respect to tapering, we algorithmically agree but conceptually disagree with Sun (1998, 2000). As opposed to him, we do not think the taper function should be conceived of as a part of the weight function because of the following reasons: Firstly, in kinematic Kirchhoff migration schemes there exist no true-amplitude weight functions. However, taper functions are still required to obtain a high-quality migration result with reduced artifacts. Secondly, there are *two* taper functions that need to be applied. One serves to avoid the aperture

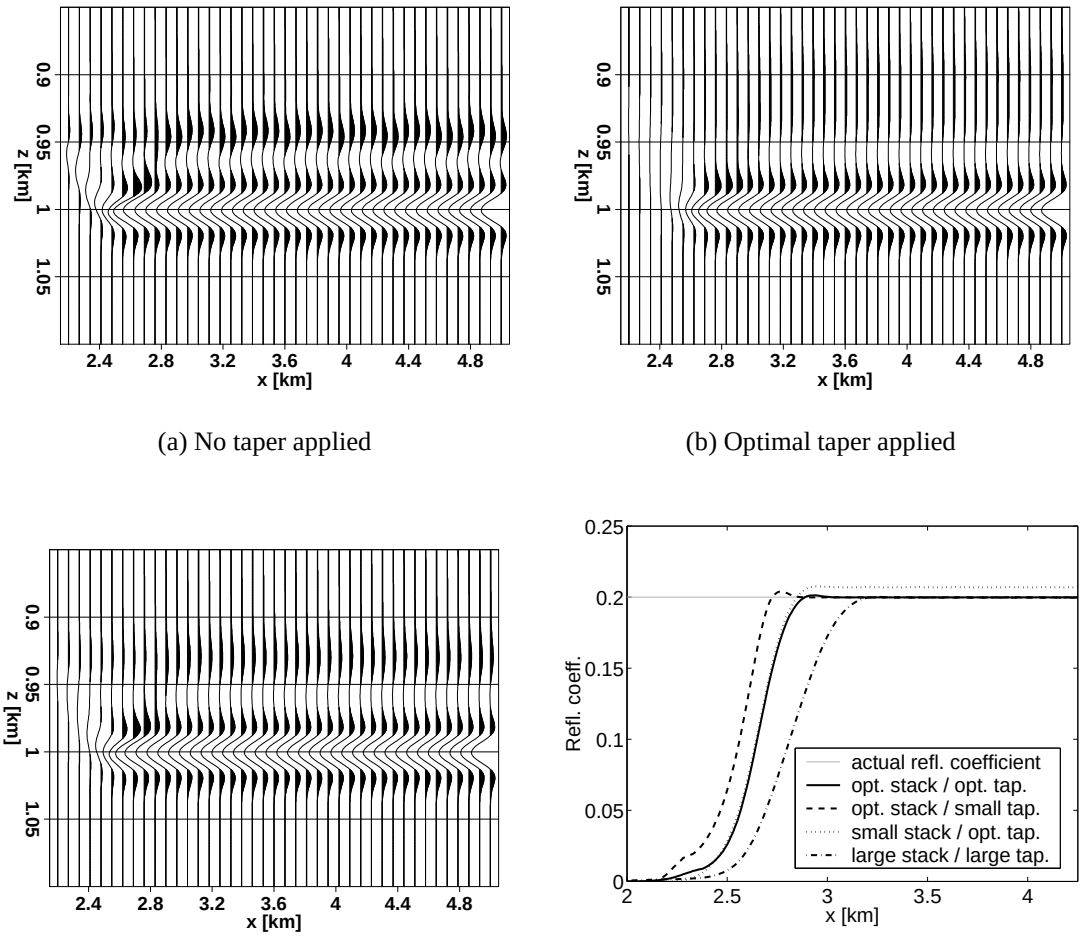

(a) No taper applied

(b) Optimal taper applied

(c) Taper too small

(d) Amplitude comparison

Figure 7: Effects of tapering. (a) Migration result without applying a taper function at all. (b) Migration result with taper function applied according to eq. (9). (c) Migration result with a taper function that is too small. (d) Amplitude comparison of different migration results with optimal and smaller/larger aperture/taper region, respectively.

effect of the limited survey area. This taper is completely independent of any weight function and applied directly to the input data before migration. The second taper is applied to the operator during migration and may be implemented as a part of the weight function. We prefer, however, to think of the true-amplitude weight and the taper functions as different concepts, even though we keep in mind that they may be combined in practice to speed up the algorithm.

CONCLUSION

Artifacts known in Kirchhoff migration as “migration noise”, “migration boundary effects” or “diffraction smiles” can be mathematically explained by means of the Method of Stationary Phase. In this paper, we have provided a more physical explanation of these effects by discussing the constructive and destructive interference of the stack in simple geometrical situations. This helps to relate the terms of the stationary-phase approximation with the actually observed migration artifacts. It turned out that, for practical applications, one has to distinguish between two principal

types of artifacts. These are

- boundary effects due to a limited survey aperture, and
- artifacts due to a limited migration operator.

Both types of artifacts are mathematically equivalent and can be explained by means of the boundary terms that result from the stationary-phase analysis of the migration integral. As predicted by the Method of Stationary Phase, the principal migration artifacts in 2.5-D exhibit a $1/\sqrt{\omega}$ decay as compared to the reflector image.

Based on our geometrical analysis, we had a closer look at a well-known way to avoid the aperture effects: tapering. The most important question with respect to tapering is how to determine the taper region. Too small a region won't suppress the effects while too large a region will destroy more information than necessary. We have shown that the ideal taper region is closely connected to the minimum aperture. Schleicher et al. (1997) have derived the minimum aperture for a dynamically correct migration to be the first projected Fresnel zone (Hubral et al., 1993) around the specular point. Sun (1998) has demonstrated that the same minimum aperture of the size of the first projected Fresnel zone is sufficient to separate the operator-end effect from the desired image. We have confirmed both observations numerically. Moreover, to get rid of the operator-end effect, a taper region of the size of the second projected Fresnel zone should be added to the operator. In principle, the projected Fresnel zone(s) can be determined during migration, even in inhomogeneous media, from dynamic ray quantities. However, to speed up the process, it is often useful to fix the operator size beforehand. Then, the constant-velocity formula should help to get an idea of an adequate aperture and taper region.

ACKNOWLEDGEMENTS

The authors thank Norman Bleistein for his careful reading and constructive criticism of the manuscript. This work was kindly supported in part by the Research Foundation of São Paulo (FAPESP), Brazil, the Brazilian National Research Council (CNPq), the Deutsche Forschungsgemeinschaft (grant Ka-1347), and the sponsors of the Wave Inversion Technology (WIT) Consortium, Karlsruhe, Germany.

REFERENCES

Abma, R., Sun, J., and Bernitsas, 1999, Antialiasing methods in Kirchhoff migration: Geophysics, **64**, no. 6, 1783–1792.

Bleistein, N., Cohen, J., and Stockwell, Jr., J., 2001, Mathematics of Multidimensional Seismic Imaging, Migration, and Inversion: Springer-Verlag Inc., New York.

Bleistein, N., 1984, Mathematical methods for wave phenomena: Academic Press Inc., Orlando.

Červený, V., and Soares, J., 1992, Fresnel volume ray tracing: Geophysics, **57**, 902–915.

Červený, V., 2001, Seismic Ray Theory: Cambridge University Press, Cambridge.

Hagedoorn, J., 1954, A process of seismic reflection interpretation: Geophys. Prosp., **2**, no. 2, 85–127.

Hubral, P., Schleicher, J., Tygel, M., and Hanitzsch, C., 1993, Determination of Fresnel zones from traveltime measurements: Geophysics, **58**, no. 5, 703–712.

Newman, P., 1975, Amplitude and phase properties of a digital migration process: Presented at the 37th Ann. Internat. Mtg., Europ. Assoc. Expl. Geoph., (Republished in: First Break, **8**, 397–403, 1990).

Schleicher, J., Hubral, P., Tygel, M., and Jaya, M., 1997, Minimum apertures and Fresnel zones in migration and demigration: Geophysics, **62**, no. 1, 183–194.

Schneider, W., 1978, Integral formulation for migration in two and three dimensions: Geophysics, **43**, no. 1, 49–76.

Stamnes, J., 1986, Waves in Focal Regions: Adam Hilger, Bristol and Boston.

Sun, S., and Bancroft, J., 2001, How much does the migration aperture actually contribute to the migration result?: Annual SEG Meeting, Expanded Abstracts.

Sun, J., 1998, On the limited aperture migration in two dimensions: Geophysics, **63**, no. 3, 984–994.

Sun, J., 2000, Limited aperture migration: Geophysics, **65**, no. 2, 584–595.

Tygel, M., Schleicher, J., and Hubral, P., 1995, Dualities between reflectors and reflection-time surfaces: Journal of Seismic Exploration, **4**, no. 2, 123–150.

Tygel, M., Schleicher, J., and Hubral, P., 1996, A unified approach to 3-D seismic reflection imaging, Part II: Theory: Geophysics, **61**, no. 3, 759–775.

Yilmaz, Ö., 2001, Seismic Data Analysis: Soc. Expl. Geophys., Tulsa.

APPENDIX A
STATIONARY-PHASE EVALUATION

In this Appendix, we shortly summarize the evaluation of integral (5) by means of the Method of Stationary Phase. For simplicity, we assume that there is only one simple point of stationary phase, denoted by ξ^*, in the integration interval (a, b). Here, "simple" means that the second derivative of q at ξ^* does not vanish, i.e., $q''(\xi^*) \neq 0$. Of course, it also must not become prohibitively small. For more than one point of stationary phase, additional integral limits are introduced, separating $I(\omega)$ into several integrals with one point ξ^* each. Then, the same analysis provides the sum of contributions from these points, provided they are *isolated* from each other, i.e., each being located outside the first Fresnel zone of the others. If this is not the case, $q''(\xi^*)$ will become too small. For details about these conditions, please refer to Bleistein (1984).

Since we expect the main contribution to integral (5) to stem from the vicinity of ξ^*, we expand $f(\xi)$ and $q(\xi)$ in Taylor series up to second order at ξ^*, where we know that $q'(\xi^*) = 0$. This approximates the integral (5) by a sum of three integrals,

$$\begin{aligned} I(\omega) \;\simeq\; & f(\xi^*)e^{i\omega q(\xi^*)} \underbrace{\int_a^b e^{i\alpha(\xi-\xi^*)^2} d\xi}_{I_0(\alpha)} \;+\; f'(\xi^*)e^{i\omega q(\xi^*)} \underbrace{\int_a^b (\xi-\xi^*) e^{i\alpha(\xi-\xi^*)^2} d\xi}_{I_1(\alpha)} \\ & + \;\frac{1}{2} f''(\xi^*)e^{i\omega q(\xi^*)} \underbrace{\int_a^b (\xi-\xi^*)^2 e^{i\alpha(\xi-\xi^*)^2} d\xi}_{I_2(\alpha)} , \quad \text{where } \alpha = \frac{\omega}{2}\frac{d^2q}{d\xi^2}\bigg|_{\xi^*} . \end{aligned} \tag{A-1}$$

The quality of this approximation is illustrated in Figure 1(a). Note that in the center part, where we expect the main contribution to integral (5), the coincidence is almost perfect. We remark that at non-simple stationary points, i.e., where $q''(\xi^*) = 0$, this approach will not work. In this case, the Taylor series for q and f have to be continued up to the order of the first non-vanishing derivative of q. If q is constant or zero, integral (5) is no longer of oscillatory character and cannot be treated by the Method of Stationary Phase.

As opposed to the integral in equation (5), integrals I_0, I_1, and I_2 in equation (A-1) *can* be solved analytically.

Integral I_1 is the one that is solved most easily. It yields

$$I_1(\alpha) = \frac{1}{2i\alpha} \int_a^b \frac{d}{d\xi} e^{i\alpha(\xi-\xi^*)^2} d\xi = \frac{1}{2i\alpha} \left[e^{i\alpha(\xi-\xi^*)^2} \right]_a^b , \tag{A-2}$$

where $\alpha \neq 0$ because of the condition that the stationary point must be isolated and simple, i.e., $q''(\xi^*) \neq 0$. We see that I_1 contains only contributions from the boundaries of the integration interval. Integral I_2 is immediately known once I_0 is determined since it is related to the latter as

$$I_2(\alpha) = \frac{1}{i} \int_a^b \frac{d}{d\alpha} e^{i\alpha(\xi-\xi^*)^2} d\xi = \frac{1}{i} \frac{dI_0(\alpha)}{d\alpha} . \tag{A-3}$$

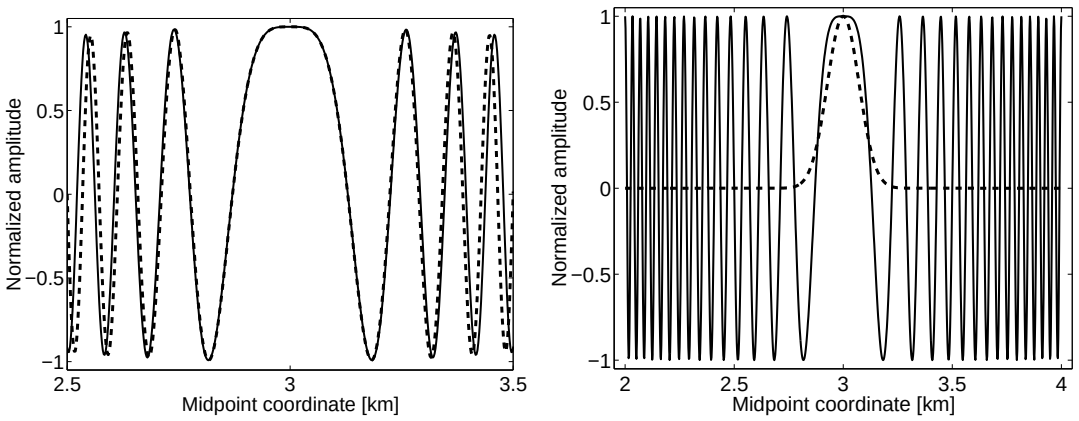

(a) (b)

Figure A-1: (a) Quality of the approximation of the integrand of equation (5) by a second-order Taylor series expansion. Shown are the real parts of the integrand function (solid line) and its approximation using second-order Taylor expansions of phase and amplitude (dashed line), central part. (b) Real part of the oscillating (solid line) and bell-shaped (dashed line) integrand functions of the integrals in equation (A-7).

The Fresnel integral I_0 requires the most extensive analysis. To study its integral limits separately, we subdivide it again into a sum of three integrals,

$$I_0(\alpha) = \int_{-\infty}^{\infty} e^{i\alpha(\xi-\xi^*)^2} d\xi - \int_{-\infty}^{a} e^{i\alpha(\xi-\xi^*)^2} d\xi - \int_{b}^{\infty} e^{i\alpha(\xi-\xi^*)^2} d\xi \ . \tag{A-4}$$

In case the stationary point is at (or very close to) one of the integral boundaries a or b, the corresponding one of the above boundary integrals is eliminated and the first integral is carried out from ξ^* to infinity.

Since the phase function is monotonic in the two boundary integrals, a transformation of variables $(\xi - \xi^*)^2 = u$ and subsequent repeated partial integration yields a power series in $1/\alpha$ (or $1/\omega$), the leading terms of which are

$$\int_{-\infty}^{a} e^{i\alpha(\xi-\xi^*)^2} d\xi \simeq \frac{1}{2i\alpha} \ \frac{1}{(a-\xi^*)} e^{i\alpha(a-\xi^*)^2} \ , \tag{A-5}$$

and

$$\int_{b}^{\infty} e^{i\alpha(\xi-\xi^*)^2} d\xi \simeq -\frac{1}{2i\alpha} \ \frac{1}{(b-\xi^*)} e^{i\alpha(b-\xi^*)^2} \ . \tag{A-6}$$

For non-isolated points of stationary phase, the distance between ξ^* and at least one of the integral boundaries is too small, such that the corresponding approximation (A-5) or (A-6) is not valid.

The integrals in equations (A-5) and (A-6) are the boundary contributions to I_0. The remaining integral describes the contribution from the point of stationary phase. A detailed analysis in the

complex plane (see, e.g., Stamnes, 1986) shows that

$$\int_{-\infty}^{\infty} e^{i\alpha(\xi-\xi^*)^2} d\xi \;=\; \frac{1+i\,\mathrm{sgn}\,\alpha}{\sqrt{2}} \int_{-\infty}^{\infty} e^{-|\alpha|\xi^2} d\xi = \sqrt{\frac{\pi}{|\alpha|}}\; e^{i\frac{\pi}{4}\,\mathrm{sgn}\,\alpha} = \sqrt{\frac{\pi}{-i\alpha}}\;, \qquad \text{(A-7)}$$

with the definition of the complex square root

$$\sqrt{z} = \sqrt{|z|}\exp\{i\arg(z)/2\}\;, \qquad -\pi < \arg(z) \le \pi\;. \qquad \text{(A-8)}$$

By symmetry, the left-hand-side integral in equation (A-7) yields exactly half this contribution if its lower limit is ξ^*.

Figure 1(b) visualizes the above identity (A-7). The real part of the oscillating function $e^{i\alpha(\xi-\xi^*)^2}$, and the bell-shaped function $e^{-|\alpha|\xi^2}$ are the solid and dashed curves, respectively. Note that equation (A-7) states that integrations from minus infinity to infinity over the two curves in Figure 1(b) yield identical results, except for a factor $1/\sqrt{2}$, or, considering also the imaginary parts, $e^{i\frac{\pi}{4}\,\mathrm{sgn}\,\alpha}$.

Combining equations (A-5) to (A-7), we obtain for I_0 up to the first order in α^{-1}

$$I_0(\alpha) \simeq \sqrt{\frac{\pi}{-i\alpha}} + \frac{1}{2i\alpha}\;\left(\frac{1}{b-\xi^*}e^{i\alpha(b-\xi^*)^2} - \frac{1}{a-\xi^*}e^{i\alpha(a-\xi^*)^2}\right)\;. \qquad \text{(A-9)}$$

By equation (A-3), this yields for I_2 up to the first order in α^{-1}

$$I_2 \simeq \frac{1}{2i\alpha}\;\left((b-\xi^*)e^{i\alpha(b-\xi^*)^2} - (a-\xi^*)e^{i\alpha(a-\xi^*)^2}\right) \qquad \text{(A-10)}$$

In other words, like I_1, I_2 also describes only contributions from the boundaries of the integration interval to that order. Collecting the terms of equation (A-1) and recognizing the Taylor expansions of $\dfrac{dq}{d\xi}$ and $f(\xi)$, we finally find

$$I(\omega) \;\simeq\; f(\xi^*)e^{i\omega q(\xi^*)}\sqrt{\frac{2\pi}{-i\omega q''(\xi^*)}} + \frac{1}{i\omega}\left[\frac{f(b)}{q'(b)}e^{i\omega q(b)} - \frac{f(a)}{q'(a)}e^{i\omega q(a)}\right]\;, \qquad \text{(A-11)}$$

where the prime denotes the derivative with respect to ξ. Under the assumption of a single, isolated point of stationary phase, the above analysis of the migration integral (4) by means of the Method of Stationary Phase has shown that its first two terms in equation (A-11) are of the order $1/\sqrt{\omega}$ and $1/\omega$, respectively. If the stationary point coincides with one of the boundaries, i.e., if $q'(a) = 0$ or $q'(b) = 0$, equation (A-11) has to slightly modified. The corresponding boundary contribution at a or b is eliminated and the leading term is divided by 2, as already indicated in the context of equations (A-4) and (A-7).

APPENDIX B
PROJECTED FRESNEL ZONE

In this Appendix, we derive expression (9) for the projected Fresnel zone in the zero-offset configuration, assuming a plane reflector with dip θ and a constant background velocity v (see Figure B-1). The projected Fresnel zone is defined as the projection of the true Fresnel zone in depth along neighboring reflection rays into the earth's surface (Hubral et al., 1993). In other words, the projected Fresnel zone ends where the ray reflected at the endpoint of the true Fresnel zone reaches the earth's surface.

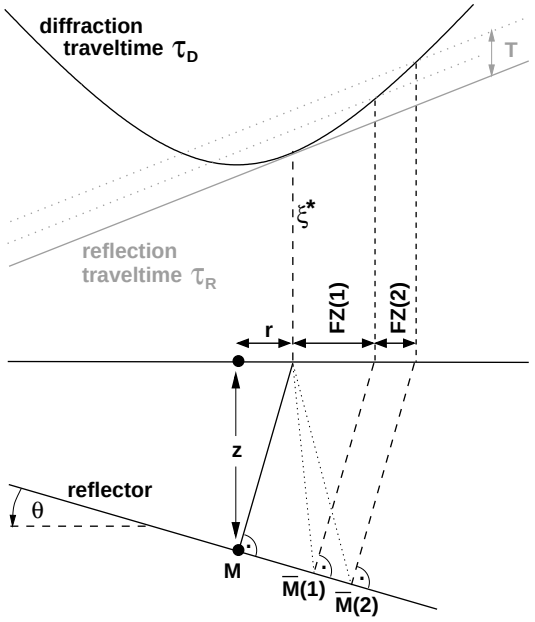

Figure B-1: Construction of the projected Fresnel zone.

We start from the definition of the Fresnel zone, equation (6). At ξ^*, the reflection traveltime, τ_R, of the normal ray reflected at M (see Figure B-1), is

$$\tau_R = \frac{2}{v}\sqrt{r^2 + z^2}\ , \tag{B-1}$$

where r is given by equation (8). The diffraction traveltime of a point $\overline{M}(n)$, also measured at ξ^*, is

$$\tau_D = \frac{2}{v}\sqrt{r^2 + z^2 + \ell(n)^2}\ , \tag{B-2}$$

where $\ell(n)$ is the distance between M and $\overline{M}(n)$. Substituting these two expressions for τ_R and τ_D in equation (6) and solving for $\ell(n)$, one finds

$$\ell(n) = \sqrt{\left(\frac{vnT}{4}\right)^2 + \frac{vnT}{2}\sqrt{r^2 + z^2}} = \sqrt{\left(\frac{vnT}{4}\right)^2 + \frac{vnTz}{2\cos\theta}}\ . \tag{B-3}$$

This is the size of the true Fresnel zone at the reflector in depth. To obtain the size of the projected Fresnel zone, we still have to project this distance into the earth's surface along neighboring normal rays (dashed rays in Figure B-1). Since these rays are parallel, the projection provides an additional division by $\cos\theta$, thus yielding formula (9).

List of Figures